DR. CLAUDIA BREGONZIO (Orcid ID : 0000-0003-3542-2177)

Article type : Research Report

Proposed Journal section:

Title: Angiotensin II modulates amphetamine-induced glial and brain vascular responses**,** and attention deficit via Angiotensin Type 1 receptor: evidence from brain regional sensitivity to amphetamine.

Author names and affiliations:

Natalia Andrea Marchese[a], Victoria Belén Occhieppo[a], Osvaldo Martin Basmadjian[a], Brenda Solange Casarsa[b], Gustavo Baiardi[b] and[*]Claudia Bregonzio[a].

[a]Instituto de Farmacología Experimental Córdoba (IFEC-CONICET) Departamento de Farmacología. Facultad de Ciencias Químicas Universidad Nacional de Córdoba, Córdoba, Argentina.

[b]Laboratorio de Neurofarmacología, (IIBYT-CONICET) Universidad Nacional de Córdoba Facultad de Ciencias Químicas, Universidad Católica de Córdoba, Córdoba, Argentina.

Corresponding author: Claudia Bregonzio PhD

e-mail address: bregonzio@fcq.unc.edu.ar

Phone: 54-351-5353159

Address: Instituto de Farmacología Experimental Córdoba (IFEC-CONICET) Departamento de Farmacología. Facultad de Ciencias Químicas Universidad Nacional de Córdoba. Haya de la Torre S/N, esquina Medina Allende. Edificio Nuevo de Ciencias I Ciudad Universitaria Córdoba,

This article has been accepted for publication and undergone full peer review but has not been through the copyediting, typesetting, pagination and proofreading process, which may lead to differences between this version and the Version of Record. Please cite this article as doi: 10.1111/EJN.14605

Argentina.

Running title: AT_1-R and amphetamine-induced alterations

Total number of pages: 26

Total number of figures: 9 (2 supplementary figures)

Total number of tables: 1

Total number of equations: 0

Total number of words in the manuscript: 5375

Total number of words in the abstract: 250

Key words: astrocytes; microglia; brain microvessels; attention deficit; prefrontal cortex

Abbreviations: Amph (Amphetamine); DA (Dopamine); CNS (Central Nervous System); HSP (Heat Shock Protein); PFC (Prefrontal Cortex); HPC (Hippocampus); AngII (Angiotensin II); AT_1-R (Angiotensin Type 1 Receptor); ROS (Reactive Oxygen Species); SHR (Spontaneous Hypertensive Rats); NO (Nitric Oxide); CV (Candesartan); Veh (Vehicle); Sal (Saline); PB (Phosphate Buffer); PBS (Phosphate-Buffered Saline); GFAP (Glial Fibrillary Acidic Protein); NGS (Normal Goat Serum); ABC (Avidin-Biotin-peroxidase Complex); TBS (Tris-Buffered Saline); MDA (malondialdehyde); TBA (thiobarbituric acid)

Abstract

Amphetamine-induced neuroadaptations involve vascular damage, neuroinflammation, a hypo-functioning prefrontal cortex (PFC) as well as cognitive alterations. Brain angiotensin II, through Angiotensin Type 1 receptor (AT_1-R), mediates oxidative/inflammatory responses, promoting endothelial dysfunction, neuronal oxidative damage and glial reactivity. The present work aims to unmask the role of AT_1-R in the development of amphetamine-induced changes over glial and vascular components within PFC and hippocampus. Attention deficit was evaluated as a behavioral neuroadaptation induced by amphetamine. Brain microvessels were isolated to further evaluate vascular alterations after amphetamine exposure. Male Wistar rats were administered with AT_1-R antagonist, Candesartan, followed by repeated amphetamine. After one week drug-off period, animals received a saline or amphetamine challenge and were evaluated in behavioral tests. Afterwards, their brains were processed for cresyl violet staining, CD11b (microglia marker), GFAP (astrocyte marker) or von Willebrand factor (vascular marker) immunohistochemistry, and oxidative/cellular stress determinations in brain microvessels. Statistical analysis was performed by using Factorial ANOVA followed by Bonferroni or Tukey tests. Repeated amphetamine administration increased astroglial and microglial markers immunoreactivity, increased apoptotic cells and promoted vascular network rearrangement at the PFC concomitantly with an attention deficit. Although, the amphetamine challenge improved the attentional performance, it triggers detrimental effects probably because of the exacerbated malondialdehyde levels and increased heat shock protein 70 expression in microvessels. All observed amphetamine-induced alterations were prevented by the AT_1-R blockade. Our results support the AT_1-R involvement in the development of oxidative/inflammatory conditions triggered by amphetamine exposure, affecting cortical areas and increasing vascular susceptibility to future challenges.

Introduction

Amphetamines constitute a group of drugs associated with clinical use and illicit consumption, being D-Amphetamine (Amph) the simplest compound presenting all the chemical properties that underlie their physiological actions (Berman *et al.*, 2009; Carvalho *et al.*, 2012). In rodents, Amph has long been used as a pharmacological tool to promote dopamine (DA)-imbalance which modifies future responses to pharmacological and environmental stimuli (Kalivas, 2007). Currently, these neuroadaptations -including cellular, molecular and metabolic modifications- are considered to take place along with neuroinflammation (Clark *et al.*, 2013; Loftis & Janowsky, 2014). Within the central nervous system (CNS), astrocytes, microglia and endothelial cells sense disturbed neuronal activity following injury, disease or neurotoxic agents (Clark *et al.*, 2013; Shaerzadeh *et al.*, 2018). Besides the increase in DA neurotransmission, in brain areas receiving dopaminergic inputs, Amph promotes astrocyte reactivity stimulating cytokine production (Kadota & Kadota, 2004; Vicente-Rodriguez *et al.*, 2016; Du *et al.*, 2017; Shah *et al.*, 2012). Furthermore, microglial activation has been proposed as a hallmark for Amph derivatives-induced neurotoxicity (Thomas *et al.*, 2004), while gene and protein analyses in microglial cells indicate increased cytokine production and nitrosative stress after Amph exposure (Tocharus *et al.*, 2008; Wisor *et al.*, 2011). At vascular level, increased pro-inflammatory markers, oxidative stress, and heat shock proteins expression were reported in meninges-associated vasculature of rodents 24h after non-toxic doses of Amph (Thomas *et al.*, 2009; Thomas *et al.*, 2010). Interestingly, chronic methylphenidate -at an equivalent clinical dosage used to treat attention deficit in humans- promotes vascular, glial and neuronal changes in rats (Coelho-Santos *et al.*, 2019).

Altered brain connectivity and neuropsychiatric impairments associated with Amph depend on the administration schedule and off-drug periods, showing regional sensitivity and time-dependent characteristics (Berman *et al.*, 2008; Shaerzadeh *et al.*, 2018). Compelling evidence indicates that decreased neuronal integrity and compromised glial activity in prefrontal cortex (PFC) are a common hallmark among Amph users (Sailasuta *et al.*, 2010; Mackey & Paulus, 2013). Furthermore, cell death, loss of dopaminergic endings and elevated levels of pro-inflammatory markers, were reported in limbic areas -including PFC- after chronic Amph exposure in rodents (Kim & Mandyam, 2014; Valvassori *et al.*, 2015). Indeed, cortical alterations involving inflammation, oxidative stress, and hypo-perfusion have been associated with mood disorders and attention deficits observed after prolonged Amph consumption (Ornstein *et al.*, 2000; Downey &

Loftis, 2014). Nevertheless, hippocampus (HPC) -implicated in spatial navigation and cognitive processes- also displays neurovascular and glial alterations after Amph exposure (Che *et al.*, 2013; de Souza Gomes *et al.*, 2015; Coelho-Santos *et al.*, 2019).

In the last decades, brain Angiotensin II (AngII) has come into focus as a pleiotropic system through Angiotensin Type 1 receptor (AT_1-R) activation. In pathological conditions, AT_1-R expressed in astrocytes, microglia and brain endothelial cells emerge as key mediator in the development of an oxidative/inflammatory microenvironment and glial activation (Zhou *et al.*, 2005; von Bohlen und Halbach & Albrecht, 2006). In this sense, glial reactivity elicited by LPS in cell cultures, involves the activation and up-regulation of AT_1-R, NFκB signaling, further production of cytokines and reactive oxygen species (ROS) (Bhat *et al.*, 2016). In the spontaneously hypertensive rats (SHR) strain, the AT_1-R overexpression in brain microvessels is consistent with vascular oxidative stress and inflammation (Zhou *et al.*, 2005). In this scenario, AT_1-R mediates nitric oxide (NO) imbalance (Yamakawa *et al.*, 2003), vascular increased permeability and inflammatory cells recruitment and activation (Ando *et al.*, 2004a; Ando *et al.*, 2004b). Particularly, AT_1-R promotes the initiation and progression of local brain inflammatory and oxidative responses under DA-imbalance conditions, as described in animal models of senescence (Labandeira-Garcia *et al.*, 2011) and Parkinson's disease (Labandeira-Garcia *et al.*, 2012).

Our previous reports support the AT_1-R involvement in the development of Amph-induced neuroadaptations at neurochemical, structural and behavioral levels (Paz *et al.*, 2011; Paz *et al.*, 2013; Occhieppo *et al.*, 2017). Moreover, a long-lasting overexpression of functional AT_1-R was observed in DA-innervated areas after Amph exposure (Paz *et al.*, 2014), whereas altered AT_1-R functionality was described regarding classical AngII-elicited actions (Casarsa *et al.*, 2015). In the present study, we aimed to characterize the pattern of Amph-induced deleterious effects, over microglia and astrocyte activation along with vascular network organization in PFC and HPC; and how the AT_1-R modulates those effects. Additionally, Amph-induced oxidative and cellular stress responses were studied in isolated brain microvessels. Moreover, behavioral tests were performed to assess attentional deficit as a functional outcome of PFC activity, which is considered as the main cognitive alteration associated with Amph exposure.

Materials and methods

Animals

Adult male Wistar rats (250–320g), from the Department of Pharmacology vivarium (Facultad de Ciencias Químicas, Universidad Nacional de Córdoba, Argentina), were randomly housed in groups of four one week before the beginning of the experimental protocol. Throughout the experiment, animals were maintained at controlled environmental conditions (20–24°C, 12h light/dark cycle with lights on at 07 a.m.) with free access to food and water.

All procedures were approved by Animal Care and Use Committee of the Facultad de Ciencias Químicas, Universidad Nacional de Córdoba, Argentina (Res nº 46/15), in accordance with the NIH Guide for the Care and Use of Laboratory Animals.

Drugs

The selective AT_1-R antagonist, Candesartan cilexetil (CV, Laboratorios Phoenix, Buenos Aires, Argentina), was dissolved in 0.1N NaHCO3 (vehicle, Veh). D-amphetamine sulfate (Amph) was dissolved in 0.9% NaCl (saline, Sal) immediately before use. The selected doses were chosen considering previous works (Marchese *et al.*, 2016).

Experimental design

In order to evaluate the involvement of AT_1-R in the development of Amph-induced long-term effects, the animals received oral administration of Veh/CV (3mg/kg by gavage, using a feeding needle) once a day during 5 days. From day 6 to day 10, they were daily injected with Sal/Amph (2.5mg/kg i.p.) and left undisturbed in their home cages for a drug-free period of 1 week until the day of the experiment. Then, four groups were conformed: Veh-Sal; Veh-Amph; CV-Sal and CV-Amph. On day 17, the animals were tested for behavioral performance after a Sal/Amph (0.5mg/kg i.p) challenge and brain samples were taken for immunohistochemistry or cresyl violet staining. Additionally, brain microvessels were isolated at day 17 to evaluate the putative oxidative and cellular stress evidenced by the Amph challenge (saline i.p., Sal, was considered for basal responses).

Immunohistochemistry

GFAP and CD11b immunohistochemistry

Animals were anesthetized with chloral hydrate (400mg/kg i.p.) and transcardially perfused with 200ml of saline and heparin (200µl/l), followed by 250 ml of 4% paraformaldehyde in 0.1M Phosphate-Buffer (PB, pH 7.4). Brains were removed and then stored at 4°C in a 30% sucrose solution. Coronal sections of 20µm were cut using a freezing microtome (Leica CM1510S), and collected in 0.01M Phosphate-Buffered Saline (PBS, pH 7.4). They were placed in a mixture of

10% H_2O_2 and 10% methanol for 2h and then incubated in 10% Normal Goat Serum (NGS; Natocor, Córdoba, Argentina) in 0.1M PBS for 2h, to block nonspecific binding sites. The free-floating sections were incubated overnight, at room temperature, with: mouse monoclonal anti-Glial Fibrillary Acidic Protein (GFAP) (1:1000; Sigma-Aldrich, MO, USA) or mouse monoclonal anti-CD11b (1:1000; Millipore, CA, USA). The next day, the sections were rinsed with 0.01M PBS and incubated with biotin-labeled goat anti-mouse secondary antibody (Jackson Immune Research, Laboratories Inc, PA, USA) diluted 1:3000 in 2% NGS-0.1M PBS, and Avidin-Biotin-peroxidase Complex (ABC-Vector Laboratories, CA, USA) for 2h each one, at room temperature. The peroxidase label was detected with diaminobenzidine hydrochloride (Sigma-Aldrich, MO, USA) and hydrogen peroxide; the solution was intensified with 1% cobalt chloride and 1% nickel ammonium sulfate. Finally, the free-floating sections were mounted on gelatinized slides, air-dried overnight, dehydrated, cleared in xylene, and placed under a cover slip with DPX mounting medium (Flucka Analytical).

von Willebrand Factor immunohistochemistry

Animals were sacrificed by decapitation and their brains were removed, snap-frozen and stored at -70°C until use. Coronal sections of 40µm were cut using the freezing microtome, mounted on gelatinized slides and fixed with methanol (15 min at -20ºC). They were placed in a mixture of 10% H_2O_2 and 10% methanol for 2h and, after 3 washes in 0.01M Tris-Buffered Saline (TBS), the samples were incubated in 10% NGS in 0.1M TBS for 2h. Mounted sections were incubated overnight with a rabbit anti-von Willebrand factor antibody (Dako Denmark A/S), diluted 1:200 in 0.1M TBS, containing 2% NGS and 0.3% Triton X-100 (Flucka Analytical). Then, they were incubated with biotin-labeled anti-rabbit secondary antibody (Vector Laboratories, CA, USA) diluted 1:500 in 2% NGS-0.1M TBS; and later with ABC, diluted 1:200 in 2% NGS-0.1M TBS, for 2h each at room temperature. The peroxidase label was detected as above mentioned and the mounted sections were air-dried overnight, dehydrated, cleared in xylene, and placed under a cover slip with DPX mounting medium.

Cresyl violet staining

Coronal sections of 20µm were collected simultaneously from brains used for immunohistochemistry. Slices were mounted on gelatinized slides and air-dried overnight. To rehydrate, the mounted sections were dipped in distilled water for 10min. Samples were stained with cresyl violet (Sigma-Aldrich, MO, USA) for 2min and dipped in water. After staining, slides were sequentially dipped into 70% alcohol (2min), acetic acid-96% alcohol mixture (2min), 96%

alcohol (1min) and 100% alcohol (1min). Finally, the mounted sections were air-dried overnight, dehydrated and cleared in xylene, and placed under a cover slip with DPX mounting medium.

Brain microvessels determinations

Isolation of brain microvessels

The procedure was performed as described elsewhere by other authors (Zhou *et al.*, 2005). Briefly, animals were anesthetized with chloral hydrate (400mg/kg i.p.) and perfused with 30 ml of saline. Brains were removed discarding cerebellum, rinsed and homogenized. The homogenate was centrifuged twice at 1000g for 10 min, with 3 volumes of cold isotonic sucrose buffer (0.32mol/L sucrose, 3mmol/L HEPES in PBS, pH 7.4) each time and the supernatants in-between were discarded. Then, the precipitate was re-suspended in sucrose buffer and centrifuged twice for 30 sec. at 100g. The supernatants were pooled, washed twice with sucrose buffer and once with 0.1% bovine serum albumin in PBS at 200g for 2min each step. Finally, the pellet was re-suspended in 0.1% bovine serum albumin in PBS and centrifuged at 14000g for 10min and precipitate was stored at −70°C until use. This technique allows the isolation of small-caliber vessels that are mainly constituted only by endothelial cells.

Immunofluorescence

Brain microvessels were mounted on microscope slides positive charged under a magnifying glass and dried at 37ºC. The following steps were carried out on a wet chamber and sheltered from light. Microvessels were exposed to 1% bovine serum albumin in PBS for 1h, rinsed twice and incubated overnight at 4ºC with: mouse monoclonal anti-AT_1-R (1:100, provided by Dr. Hans Imboden), or mouse monoclonal anti-heat shock protein 70 (HSP70, 1:400, Sigma-Aldrich, MO, USA). The next day, the microvessels were rinsed twice with PBS-0.05% tween followed by one rinse with PBS, 5min, and incubated for 30min at room temperature with the secondary antibody anti-mouse (1:400; Alexa Fluor 555-Abcam). Then, the microvessels were rinsed and incubated with Hoechst (1:3000) for 7min. Finally, cover-slips were placed using 90% glycerol as mounting media and images were immediately obtained.

Lipid Peroxidation

Malondialdehyde (MDA) content was determined by thiobarbituric acid (TBA) reaction as previously described (Ohkawa *et al.*, 1979). Briefly, the microvessels isolated at room temperature were resuspended in 1.15% KCl and homogenized for 10min. An aliquot was reserved for protein content determination (by Bradford assay) and 8.1% sodium dodecyl sulfate, 20% acetic acid -pH

3.5- and 0.8% TBA were added to the remaining homogenate. Samples were heated at 95ºC for 1h, cooled afterwards and centrifuged at 4000 r.p.m. The colored product absorbance at 532nm was estimated and MDA content (nmol/protein μg) was calculated. External standard of tetramethoxy-propane was used for the calibration curve.

Image processing

All the images were obtained by using a Leica DM 4000B microscope equipped with Leica FW4000 and a DFC Leica digital camera attached to a contrast enhancement device and digitalized images were stored in a computer. All the images were obtained with identical exposure times, gain and offsets, and saved in TIFF format (1392 x 1040 pixels). The images were processed using ImageJ software (U.S. National Institutes of Health, USA). The analyses were made blinded to the experimental groups.

Image quantification was performed in infra- and pre-limbic PFC (Bregma: 3.20mm) and HPC (Bregma: −3.30/−3.60 mm), which were identified and delimited according to Paxinos and Watson atlas (2009). The measurements were taken bilaterally in two sections and the final value was obtained as the average of the four counted sections. The presented results are meant to provide relative data on glial and vascular markers expression in all different experimental conditions but are not meant to be accurate estimates of absolute values.

Astrocyte reactivity by GFAP immunostaining

GFAP-stained sections were taken at 400x magnification and the area occupied by astrocytes was quantified, fixing a threshold of 120-140, and expressed as a percentage in relation to the total evaluated area.

Microglial reactivity by CD11b immunostaining

CD11b-stained sections were taken at 400x magnification and the area occupied by microglial cells was quantified, fixing a threshold of 175-200, and expressed as a percentage in relation to the total evaluated area.

Apoptotic cells by cresyl violet staining

The images were taken at 400x magnification and apoptotic cells were identified by delimited Nissl bodies' accumulation, lacking cytoplasmic volume. Their number was manually quantified and expressed relative to 0.1mm^2 of the brain area.

Vascular Network by von Willebrand Factor immunostaining

The vascular architecture analysis (200x magnification) was made as described in a previous report (Occhieppo *et al.*, 2017). Three parameters were analyzed: 1) percentage of vascular area,

2) number of branching points and 3) vessels' tortuosity, calculated as the ratio of the real distance between two consecutive branching points and the shortest distance between them (Fig. 2). This last parameter takes values from 1 to infinite, where higher values indicate a more sinuous structure.

Immunofluorescence of HSP70

Fluorescence was quantified by mean gray value, assessed at three different sections on one isolated microvessel, and its final value was calculated as follows: section's mean gray value - (background's mean gray value + 3 standard deviation of background's mean gray value); and expressed as Arbitrary Units of fluorescence intensity. The final value for each subject was the average from the measurements obtained in 6 images per rat at 400x magnification, where a maximum of 5 microvessels was analyzed in each picture. The same protocol was applied to AT_1-R quantification (Suppl. Fig 1).

Behavior

Holeboard test

The exploratory behavior was evaluated at a single-time exposure in an arena with 5 holes (arena: 60cm width x 60cm de long x 30cm de high; holes: 3cm diameter, 1 hole at the center, 4 holes in the corners separated 10cm from the wall). Behavior was recorded and the number of head dipping into each hole was quantified for 5min. The data were analyzed and shown as described previously (Baiardi *et al.*, 2007). For each animal in the experimental group, the number of visits was ordered from the most to the least visited holes. Attention deficit is considered as a significant difference between the two most explored holes.

Y-maze test

Animals were placed once at the center of a Y-shaped maze, with three equal arms (10cm width x 50cm long x 39cm tall, separated by 120º angle) and left for free exploration during 8min. The sequence of chosen entries was manually recorded and the percentage of alternations was calculated. With this purpose, three consecutive choices of three different arms were counted as an alternation, whereas the total possible alternations were calculated as the total number of entries minus 2. In this behavioral task, a lower alternation percentage is considered as an attention deficit. Animals displaying a 2min period of immobility between arms were excluded from the final analysis.

Statistical analysis

Data were analyzed using one or two-way ANOVA and reported as means ± SEM. The analysis for two-way ANOVA considered Veh/CV as *treatment* factor and Sal/Amph as *drug* factor. If interaction and/or main effect were observed, multiple comparisons were made using the Tukey's or Bonferroni's post-test. A value of $p< 0.05$ was considered significant. The analyses were performed using Graphpad Prism® 6.03 software. The artwork was conducted with Inkscape software (Free and Open Source Software licensed under the GPL).

Results

AT_1-R is involved in Amph-induced GFAP and CD11b increased expression, and vascular rearrangement in pre-limbic PFC

Amph exposure promoted glial reactivity along with neuronal apoptosis in pre-limbic PFC. Moreover, long-term vascular rearrangement was observed as increased vascular density and tortuosity, and decreased branching points in this brain area. These events were prevented by previous AT_1-R antagonism (Fig. 1 and 2).

Astrocyte reactivity was evidenced as increased GFAP-positive area in Veh-Amph group when compared to Veh-Sal group (*treatment*drug interaction* $F_{(1, 22)}=6.89$, $p= 0.015$; Bonferroni *post-hoc* $p<0.05$; Fig.1b); whereas no difference was found for CV-Amph group and control conditions. The same pattern and values were obtained after the Amph challenge, indicating no further change of astrocyte reactivity (data not shown). In the same direction, increased CD11b immunopositive area was evidenced in this brain area in Veh-Amph group, suggesting microglial reactivity after Amph exposure and its prevention by AT_1-R blockade (*treatment* $F_{(1, 25)}=6.40$ $p= 0.018$ and *drug* $F_{(1, 25)}=8.88p= 0.006$; Fig.1c).

Cresyl violet staining revealed deleterious effects of Amph exposure in this brain area as Veh-Amph group showed a significantly elevated number of apoptotic cells when compared to Veh-Sal and CV-Amph groups (*treatment* $F_{(1, 23)}=7.94p= 0.0098$, *drug* $F_{(1, 23)}=24.32p=0.0001$ and *treatment*drug interaction* $F_{(1, 23)}=15.09$ $p= 0.0007$; Bonferroni *post-hoc* $p<0.05$; Fig.1d).

When vascular network was analyzed, a vascular rearrangement was found in Veh-Amph group when compared to Veh-Sal and CV-Amph groups, evaluated by 3 parameters: **1**. percentage of vascular area (*treatment* $F_{(1, 27)}=4.51$ $p= 0.043$ and *treatment*drug interaction* $F_{(1, 27)}=11.30$ $p= 0.0023$); **2**. vessels' tortuosity (*treatment* $F_{(1, 27)}=5.88$ $p= 0.022$, *drug* $F_{(1, 27)}=5.32$ $p= 0.029$ and *treatment*drug interaction* $F_{(1, 27)}=4.48p= 0.044$); and **3**. number of branching points (*treatment*

$F_{(1, 27)}$=9.60 p= 0.0045, *drug* $F_{(1, 27)}$=7.67 p= 0.01 and *treatment*drug interaction* $F_{(1, 27)}$=4.27 p= 0.049). In all cases, Bonferroni comparison indicated p<0.05 for all parameters analyzed (Fig. 2).

Amph-induced glial and vascular alterations are region-specific

There were no changes in GFAP and CD11b immunoreactivity or vascular rearrangement in infra-limbic PFC after Amph exposure (Fig. 3). The results indicate no significant differences in the percentage of GFAP nor CD11b positive area (*treatment*drug interaction* $F_{(1, 22)}$=3.29p=0.083 and $F_{(1, 27)}$=0.05 p= 0.83, respectively). However, 24h after the Amph challenge an increased GFAP positive area in Veh-Amph group was observed compared to Veh-Sal and CV-Amph groups (*treatment*drug interaction* $F_{(1, 20)}$=7.85, p=0.011; Bonferroni *post-hoc* p<0.05, Table 1). In addition, no significant difference was observed in the percentage of vascular area of this brain area in basal conditions (*treatment*drug interaction* $F_{(1, 26)}$=2.33p= 0.14).

The analyses of HPC (Fig. 4) indicated that there were no significant differences in the percentage of GFAP nor CD11b positive area (*treatment*drug interaction* $F_{(1, 23)}$=0.00005 p= 0.99 and $F_{(1, 25)}$=0.00004 p=0.99, respectively). The same pattern and values were obtained after the Amph challenge for astrocyte reactivity (data not shown). In the same direction, in basal conditions, no significant difference was observed in the percentage of vascular area of this brain area (*treatment*drug interaction* $F_{(1, 21)}$=0.72, p= 0.40).

Amph-induced attentional deficit involves AT_1-R

The attentional deficit was observed as a lower performance in the two behavioral paradigms one week after the last Amph exposure. This deficit was not observed with the AT_1-R blocker pretreatment (Fig. **5**). Moreover, the Amph challenge masked the cognitive deficit observed in the Veh-Amph group (Fig. **6**).

For the holeboard test, there were significant differences in the head dipping into the holes ($F_{(19, 149)}$=15.15 p<0.0001). Tukey's multiple comparisons indicated that Veh-Amph was the only group that showed significant differences in the number of head dipping between the first and the second most explored holes (p<0.05). After the Amph challenge, significant differences in the head dipping into the holes were found ($F_{(19, 195)}$= 18.90 p<0.0001). However, in this case, Tukey's multiple comparisons indicated no significant differences between the first and the second most explored holes in any of the experimental groups. Additionally, the results are shown as the difference in exploration percentage between the two more explored holes (insets in Figs. 4 and 5). In this case, Veh-Amph group showed significantly higher differences than control group (Veh-

Sal) and CV pretreated animals (CV-Amph group) in basal conditions (*treatment*drug interaction* $F_{(1, 30)}$=4.50 p=0.042; Bonferroni *post-hoc* p<0.05). After the Amph challenge, no differences were found among the four experimental groups (*treatment*drug interaction* $F_{(1, 39)}$=1.25p= 0.27).

For the Y-maze test, Veh-Amph group showed a significantly lower alternation percentage than control group (Veh-Sal) and CV pretreated animals (CV-Amph group) in basal conditions (*drug* $F_{(1, 53)}$=15.02 p= 0.0003 and *treatment*drug interaction* $F_{(1, 53)}$=4.11 p= 0.048; Bonferroni *post-hoc* p<0.05). After the Amph challenge, no differences were found among the four experimental groups (*treatment*drug interaction* $F_{(1, 32)}$=0.39 p= 0.53).

Additional analyses were performed for the total activity during the behavioral test to discard motor differences among the four experimental groups (inset graphs in Fig. **5** and **6**). For the holeboard test, there were no differences in the total number of head dipping, neither for basal conditions nor after the Amph challenge (*treatment*drug interaction* $F_{(1, 30)}$=0.001 p= 0.97 and $F_{(1, 39)}$=1.16 p= 0.29, respectively). For the Y-maze test, the total arm entries showed no differences neither for basal conditions nor after the Amph challenge (*treatment*drug interaction* $F_{(1, 53)}$=0.74 p= 0.39 and $F_{(1, 32)}$=3.84 p= 0.06, respectively).

AT_1-R is involved in Amph-induced oxidative and cellular stress in brain microvessels

In brain microvessels, Amph long-term effects were observed as increased oxidative stress and cellular stress response evidenced by the Amph challenge (Fig. **7**). AT_1-R blockade prevented the development of this sensitized response.

MDA content was not different among the four experimental groups in basal conditions (*treatment*drug interaction* $F_{(1, 16)}$=1.82 p= 0.20); however, after the Amph challenge, Veh-Amph group showed significantly elevated MDA levels when compared to Veh-Sal and CV-Amph groups (*treatment* $F_{(1, 17)}$=8.31 p= 0.01, *drug* $F_{(1, 17)}$=12.19 p= 0.003 and *treatment*drug interaction* $F_{(1, 17)}$=6.52 p= 0.02; Bonferroni *post-hoc* p<0.05).

In a similar way, Amph had no effect over HSP70 expression in basal conditions (*treatment*drug interaction* $F_{(1, 15)}$=1.12 p= 0.31); whereas, after the Amph challenge, Veh-Amph group showed significantly elevated HSP70 expression when compared to Veh-Sal and CV-Amph groups (*treatment*drug interaction* $F_{(1, 15)}$=4.56 p= 0.049. Bonferroni *post-hoc* p<0.05).

Discussion

Glial reactivity and vascular network rearrangement induced by Amph exposure require AT_1-R stimulation

Our results indicate increased GFAP and CD11b positive area and apoptosis up to one week after Amph exposure in PFC (Fig. 1). Glial reactivity, observed as increased glial markers expression, has long been recognized as a specific marker for Amph toxicity (Ellison & Switzer, 1993; Thomas *et al.*, 2004). In this scenario, the transient increase in dopaminergic and glutamatergic neurotransmission has been proposed as the main effect of amphetamines' detrimental effects (Yamamoto *et al.*, 2010). Moreover, our results extend the Amph deleterious effects to the microvascular rearrangement in PFC (Fig. 2); supporting their region-specific toxicity as vascular network modifications are closely related to inflammatory processes (Costa *et al.*, 2007). Similar vascular alterations have been previously described after Amph exposure (Occhieppo *et al.*, 2017), chronic inflammatory disease (Dorr *et al.*, 2012) and schizophrenia (Katsel *et al.*, 2017).

In addition, our results show that AT_1-R is involved in the development of Amph-induced alterations in PFC, as its blockade prevented the increase in glial markers expression and the vascular rearrangement (Figs. 1-2). The role of AT_1-R in Amph-induced alterations may be attributed to its multiple actions**,** including DA neurotransmission modulation (Jiang *et al.*, 2018), dopaminergic neurons degeneration by oxidative stress, astrocyte and microglial reactivity and angiogenesis (Rodriguez-Pallares *et al.*, 2008; Rodriguez-Perez *et al.*, 2013; Labandeira-Garcia *et al.*, 2014; Jiang *et al.*, 2018). Particularly, in neuroinflammatory responses involving DA-imbalance, the brain renin-angiotensin system is considered a key mediator in triggering glial cells activation with the subsequent progression of inflammation (Dominguez-Meijide *et al.*, 2017). In the same direction, the protective effects of AT_1-R blockade have been reported for the alterations on DA neurotransmission and toxicity induced by methamphetamine (Jiang *et al.*, 2018). Considering vascular events, AngII has long been identified as a key factor in several types of angiogenesis via local AT_1-R activation and subsequent vascular endothelial growth factor synthesis and release (Greene & Amaral, 2002; Tamarat *et al.*, 2002). Although after ischemic injury, DA shows anti-angiogenic effects by decreasing AT_1-R expression and activity (Sarkar *et al.*, 2017), supporting the idea of an interplay between these two neuromodulatory systems. In this sense, blood flow regulation in PFC is highly dependent on the direct influence of DA over the local microvessels; whereas this area is the main and the first to express functional alterations during brain vascular disorders (Krimer *et al.*, 1998; Choi *et al.*, 2006).

Amph-induced alterations and AT_1-R involvement are region-specific

It is recognized that exposure to psychostimulants allows the identification of region-specific alterations (Ellison & Switzer, 1993). These alterations also include the angiotensinergic system since Amph or metamphetamine induce an increase in AT_1-R expression and activity, in specific brain areas (Paz *et al.*, 2014; Jiang *et al.*, 2018). Interestingly, Amph affected the analyzed glial and vascular components selectively in the PFC; whereas none of the studied alterations were observed at HPC (Fig. 4). Moreover, even in PFC, we found differences between pre-limbic and infra-limbic subdivisions, because only this latter showed glial reactivity after the Amph challenge (Fig. 3- table 1). In the same direction, Amph detrimental effects (regarding ROS, inflammatory cytokines and dopaminergic degeneration) were described in limbic areas, whereas they were not detected in HPC (Belcher *et al.*, 2005; Dietrich *et al.*, 2005; Tan *et al.*, 2012; Valvassori *et al.*, 2015; Jiang *et al.*, 2018). On the contrary, vascular, glial and oxidative markers increase have been described in HPC after higher doses of Amph or a very short time after the last administration (*i.e.* after 24 hs); suggesting time- and dose-dependent alterations (de Souza *et al.*, 2004; Che *et al.*, 2013; Hodes *et al.*, 2018). Since the main long-lasting effect of Amph exposure is DA neurotransmission imbalance, PFC regional susceptibility could be triggered by its greater dopaminergic innervation (Sofuoglu, 2010).

Attentional deficit induced by Amph exposure and AT_1-R role

The present study identifies an attention deficit in rats after Amph exposure concomitant with the morphological and structural changes of the non-neuronal cell types in PFC (Fig. 5). In this brain area, catecholamine neurotransmission is implicated in the coordination and integration of cues, even though they imply less complex behaviors (Jones, 2002; Arnsten, 2006). In this sense, attention is required when animals perform spatial recognition of novel environments; thus, behavioral tests evaluating exploration are indicative of PFC functional integrity, among other brain areas, such as HPC and other limbic structures (Lalonde, 2002; Dudchenko, 2004; Yabuki *et al.*, 2014). The Amph-induced working memory deficit in rodents has been previously related to oligodendrocyte altered morphology in PFC, supporting the co-existence of functional and structural alterations in this brain area after Amph exposure (Yang *et al.*, 2011). In the same direction, cortical hypo-perfusion, glial reactivity, inflammation and oxidative stress have been related to neuropsychiatric impairments in psychostimulant users, such as attention or decision-making deficits (Ornstein *et al.*, 2000; Downey & Loftis, 2014). The PFC dysfunction described long after Amph exposure is also characterized by cortical hyporeactivity, due to decreased

glutamate and DA levels together with a diminished electrical activity (Lu & Wolf, 1999; Lu *et al.*, 2010; Janetsian *et al.*, 2015). This last evidence, could explain the improvement in the attention deficit after Amph challenge obtained in the present work (Fig. 6) because Amph induces catecholamine release (Arnsten, 1998). The proposed phenomenon is in accordance with the data obtained from Amph users that show improved attentional performance after re-exposure to low doses of the stimulant (Mahoney *et al.*, 2011). Additionally, we previously showed an increased hippocampal synaptic plasticity and resistance to the interference of long-term memory consolidation by using the same experimental protocol (Marchese *et al.*, 2016).

Remarkably, AT_1-R blockade prevented the development of Amph-induced attention deficit and a similar protective effect has been described in the development of cognitive deficits (Marchese *et al.*, 2016), as well as in neuroinflammatory scenarios in different animal models (Mogi *et al.*, 2007; Sharma & Singh, 2012; Sun *et al.*, 2015); whereas a deleterious interplay between AT_1-R activation and DA degeneration takes place in the striatum (Jiang *et al.*, 2018) along with cognitive deficits in senescence (Villar-Cheda *et al.*, 2014).

Amph-induced oxidative and cellular stress in brain microvessels: AT_1-R role

In our findings, the long-term effects of Amph exposure over brain microvascular responses are observed as sensitized oxidative stress and HSP70 expression, elicited by the Amph challenge (Fig. 7). It has been previously reported that a single non-toxic dose of Amph increases the expression of inflammatory and cellular stress genes in the meninges-associated vasculature, up to 24hs after drug exposure (Thomas *et al.*, 2009; Thomas *et al.*, 2010). However, from our knowledge, no evidence has been previously reported after Amph exposure regarding sensitized oxidative/inflammatory responses in brain microvessels. Furthermore, there is an established link between elevated ROS levels and further stimulating HSP70 synthesis as a protective response to apoptotic signaling (Horowitz & Robinson, 2007; Lee *et al.*, 2015). Additionally, we found no sensitized response to the Amph challenge in brain microvessels obtained from animals pretreated with AT_1-R blocker. In complementary experiments, we found that a basal increase in AT_1-R expression might trigger the sensitized response (in brain microvessels after Amph-exposure, Suppl. Fig. 1) given that a similar increase in HSP70 levels was observed after the AngII intracerebroventricular challenge (Suppl. Fig. 2). Particularly, AT_1-R up-regulation in SHR brain microvessels has been related to increased levels of heat shock family components, pro-inflammatory mediators and endothelial imbalance of NO and ROS levels (Ando *et al.*, 2004; Zhou *et al.*, 2005).

Conclusion

Our results bring into focus a sensitized brain vascular response long after Amph exposure and support the proposal that a compromised vasculature could be involved in the deleterious conditions, described for Amph users or chronic Amph treatments (Berman *et al.*, 2009; Carvalho *et al.*, 2012). Vascular alterations are considered triggering events for several inflammatory conditions in the CNS, as they would affect local metabolic demands and neuronal functioning (Tesfamariam & DeFelice, 2007; Iadecola, 2010; El Assar *et al.*, 2013). The brain region specific long-lasting changes in glial reactivity and vascular network rearrangement could imply an increased susceptibility to local alterations. Finally, the involvement of AT_1-R in the enduring deleterious microenvironment encourages further studies focusing on AngII system in the development and progression of neuroinflammatory pathologies.

Acknowledgements

The authors are grateful to Estela Salde and Lorena Mercado for their laboratory technical assistance and Javier Reparaz for animal care support. This study was granted by Consejo Nacional de Investigaciones Científicas y Técnicas (CONICET) nº 11220120100373CO-KB1 and Secretaría de Ciencia y Técnica (SECyT- UNC) to Dr. Bregonzio.

Competing Interests

The authors declare no conflicts of interests

Author Contributions

NAM; VBO; OMB and BSC performed the experiments. NAM performed statistical analyses. GB participated in behavioral tests planning and data interpretation. NAM and CB wrote the manuscript and VBO and OMB revised the manuscript.

Data accessibility

The authors confirm that all data underlying the findings are fully available without restriction. All relevant data are within the paper.

References

Ando, H., Jezova, M., Zhou, J. & Saavedra, J.M. (2004) Angiotensin II AT1 receptor blockade decreases brain artery inflammation in a stress-prone rat strain. *Ann NY Acad Sci*, **1018**, 345-350.

Arnsten, A.F. (1998) Catecholamine modulation of prefrontal cortical cognitive function. *Trends Cogn Sci*, **2**, 436-447.

Arnsten, A.F. (2006) Stimulants: Therapeutic actions in ADHD. *Neuropsychopharmacology;* **31**, 2376-2383.

Belcher, A.M., O'Dell, S.J. & Marshall, J.F. (2005) Impaired object recognition memory following methamphetamine, but not p-chloroamphetamine- or d-amphetamine-induced neurotoxicity. *Neuropsychopharmacology*, **30**, 2026-2034.

Berman, S.M., Kuczenski, R., McCracken, J.T. & London, E.D. (2009) Potential adverse effects of amphetamine treatment on brain and behavior: a review. *Mol Psychiatry*, **14**, 123-142.

Carvalho, M., Carmo, H., Costa, V.M., Capela, J.P., Pontes, H., Remiao, F., Carvalho, F. & Bastos Mde, L. (2012) Toxicity of amphetamines: an update. *Arch Toxicol*, **86**, 1167-1231.

Costa, C., Incio, J. & Soares, R. (2007) Angiogenesis and chronic inflammation: cause or consequence? *Angiogenesis*, **10**, 149-166.

Che, Y., Cui, Y.H., Tan, H., Andreazza, A.C., Young, L.T. & Wang, J.F. (2013) Abstinence from repeated amphetamine treatment induces depressive-like behaviors and oxidative damage in rat brain. *Psychopharmacology*, **227**, 605-614.

Choi, J.K., Chen, Y.I., Hamel, E. & Jenkins, B.G. (2006) Brain hemodynamic changes mediated by dopamine receptors: Role of the cerebral microvasculature in dopamine-mediated neurovascular coupling. *NeuroImage*, **30**, 700-712.

de Souza, F.A., Sanchis-Segura, C., Fukada, S.Y., de Bortoli, V.C., Zangrossi, H., Jr. & de Oliveira, A.M. (2004) Intracerebroventricular effects of angiotensin II on a step-through passive avoidance task in rats. *Neurobiol Learn Mem*, **81**, 100-103.

Dietrich, J.B., Mangeol, A., Revel, M.O., Burgun, C., Aunis, D. & Zwiller, J. (2005) Acute or repeated cocaine administration generates reactive oxygen species and induces antioxidant enzyme activity in dopaminergic rat brain structures. *Neuropharmacology*, **48**, 965-974.

Dominguez-Meijide, A., Rodriguez-Perez, A.I., Diaz-Ruiz, C., Guerra, M.J. & Labandeira-Garcia, J.L. (2017) Dopamine modulates astroglial and microglial activity via glial renin-angiotensin system in cultures. *Brain Behav Immun*, **62**, 277-290.

Dorr, A., Sahota, B., Chinta, L.V., Brown, M.E., Lai, A.Y., Ma, K., Hawkes, C.A., McLaurin, J. & Stefanovic, B. (2012) Amyloid-beta-dependent compromise of microvascular structure and function in a model of Alzheimer's disease. *Brain*, **135**, 3039-3050.

Downey, L.A. & Loftis, J.M. (2014) Altered energy production, lowered antioxidant potential, and inflammatory processes mediate CNS damage associated with abuse of the psychostimulants MDMA and methamphetamine. *Eur J Pharmacol*, **727**, 125-129.

Dudchenko, P.A. (2004) An overview of the tasks used to test working memory in rodents. *Neurosci Biobehav Rev*, **28**, 699-709.

El Assar, M., Angulo, J. & Rodriguez-Manas, L. (2013) Oxidative stress and vascular inflammation in aging. *Free Radic Biol Med*, **65**, 380-401.

Ellison, G. & Switzer, R.C., 3rd (1993) Dissimilar patterns of degeneration in brain following four different addictive stimulants. *Neuroreport*, **5**, 17-20.

Greene, A.S. & Amaral, S.L. (2002) Microvascular angiogenesis and the renin-angiotensin system. *Curr Hypertens Rep*, **4**, 56-62.

Hodes, A., Lifschytz, T., Rosen, H., Cohen Ben-Ami, H. & Lichtstein, D. (2018) Reduction in endogenous cardiac steroids protects the brain from oxidative stress in a mouse model of mania induced by amphetamine. *Brain Res Bull*, **137**, 356-362.

Horowitz, M. & Robinson, S.D. (2007) Heat shock proteins and the heat shock response during hyperthermia and its modulation by altered physiological conditions. *Prog Brain Res*, **162**, 433-446.

Iadecola, C. (2010) The overlap between neurodegenerative and vascular factors in the pathogenesis of dementia. *Acta Neuropathol*, **120**, 287-296.

Janetsian, S.S., Linsenbardt, D.N. & Lapish, C.C. (2015) Memory impairment and alterations in prefrontal cortex gamma band activity following methamphetamine sensitization. *Psychopharmacology*, **232**, 2083-2095.

Jiang, L., Zhu, R., Bu, Q., Li, Y., Shao, X., Gu, H., Kong, J., Luo, L., Long, H., Guo, W., Tian, J., Zhao, Y. & Cen, X. (2018) Brain Renin-Angiotensin System Blockade Attenuates Methamphetamine-Induced Hyperlocomotion and Neurotoxicity. *Neurotherapeutics*, **15**, 500-510.

Jones, M.W. (2002) A comparative review of rodent prefrontal cortex and working memory. *Curr Mol Med*, **2**, 639-647.

Katsel, P., Roussos, P., Pletnikov, M. & Haroutunian, V. (2017) Microvascular anomaly conditions in psychiatric disease. Schizophrenia - angiogenesis connection. *Neurosci Biobehav Rev*, **77**, 327-339.

Krimer, L.S., Muly, E.C., 3rd, Williams, G.V. & Goldman-Rakic, P.S. (1998) Dopaminergic regulation of cerebral cortical microcirculation. *Nature Neurosci*, **1**, 286-289.

Labandeira-Garcia, J.L., Garrido-Gil, P., Rodriguez-Pallares, J., Valenzuela, R., Borrajo, A. & Rodriguez-Perez, A.I. (2014) Brain renin-angiotensin system and dopaminergic cell vulnerability. *Front Neuroanat*, **8**, 67.

Lalonde, R. (2002) The neurobiological basis of spontaneous alternation. *Neurosci Biobehav Rev*, **26**, 91-104.

Lee, J.H., Lee, Y.K., Lim, J.J., Byun, H.O., Park, I., Kim, G.H., Xu, W.G., Wang, H.J. & Yoon, G. (2015) Mitochondrial Respiratory Dysfunction Induces Claudin-1 Expression via Reactive Oxygen Species-mediated Heat Shock Factor 1 Activation, Leading to Hepatoma Cell Invasiveness. *J Biol Chem*, **290**, 21421-21431.

Lu, P., Mamiya, T., Lu, L., Mouri, A., Niwa, M., Kim, H.C., Zou, L.B., Nagai, T., Yamada, K., Ikejima, T. & Nabeshima, T. (2010) Silibinin attenuates cognitive deficits and decreases of dopamine and serotonin induced by repeated methamphetamine treatment. *Behav brain Res*, **207**, 387-393.

Lu, W. & Wolf, M.E. (1999) Repeated amphetamine administration alters AMPA receptor subunit expression in rat nucleus accumbens and medial prefrontal cortex. *Synapse*, **32**, 119-131.

Mahoney, J.J., 3rd, Jackson, B.J., Kalechstein, A.D., De La Garza, R., 2nd & Newton, T.F. (2011) Acute, low-dose methamphetamine administration improves attention/information processing speed and working memory in methamphetamine-dependent individuals displaying poorer cognitive performance at baseline. *Prog Neuropsychopharmacol Biol Psych*, **35**, 459-465.

Marchese, N.A., Artur de laVillarmois, E., Basmadjian, O.M., Perez, M.F., Baiardi, G. & Bregonzio, C. (2016) Brain Angiotensin II AT1 receptors are involved in the acute and long-term amphetamine-induced neurocognitive alterations. *Psychopharmacology*, **233**, 795-807.

Mogi, M., Tsukuda, K., Li, J.M., Iwanami, J., Min, L.J., Sakata, A., Fujita, T., Iwai, M. & Horiuchi, M. (2007) Inhibition of cognitive decline in mice fed a high-salt and cholesterol diet by the angiotensin receptor blocker, olmesartan. *Neuropharmacology*, **53**, 899-905.

Occhieppo, V.B., Marchese, N.A., Rodriguez, I.D., Basmadjian, O.M., Baiardi, G. & Bregonzio, C. (2017) Neurovascular unit alteration in somatosensory cortex and enhancement of thermal nociception induced by amphetamine involves central AT1 receptor activation. *Eur J Neurosci*.

Ornstein, T.J., Iddon, J.L., Baldacchino, A.M., Sahakian, B.J., London, M., Everitt, B.J. & Robbins, T.W. (2000) Profiles of cognitive dysfunction in chronic amphetamine and heroin abusers. *Neuropsychopharmacology*, **23**, 113-126.

Paz, M.C., Marchese, N.A., Stroppa, M.M., Gerez de Burgos, N.M., Imboden, H., Baiardi, G., Cancela, L.M. & Bregonzio, C. (2014) Involvement of the brain renin-angiotensin system (RAS) in the neuroadaptive responses induced by amphetamine in a two-injection protocol. *Behav Brain Res*, **272**, 314-323.

Rodriguez-Pallares, J., Rey, P., Parga, J.A., Munoz, A., Guerra, M.J. & Labandeira-Garcia, J.L. (2008) Brain angiotensin enhances dopaminergic cell death via microglial activation and NADPH-derived ROS. *Neurobiol Dis*, **31**, 58-73.

Rodriguez-Perez, A.I., Dominguez-Meijide, A., Lanciego, J.L., Guerra, M.J. & Labandeira-Garcia, J.L. (2013) Dopaminergic degeneration is enhanced by chronic brain hypoperfusion and inhibited by angiotensin receptor blockage. *Age*, **35**, 1675-1690.

Sarkar, C., Ganju, R.K., Pompili, V.J. & Chakroborty, D. (2017) Enhanced peripheral dopamine impairs post-ischemic healing by suppressing angiotensin receptor type 1 expression in endothelial cells and inhibiting angiogenesis. *Angiogenesis*, **20**, 97-107.

Sharma, B. & Singh, N. (2012) Experimental hypertension induced vascular dementia: pharmacological, biochemical and behavioral recuperation by angiotensin receptor blocker and acetylcholinesterase inhibitor. *Pharmacol Biochem Behav*, **102**, 101-108.

Sofuoglu, M. (2010) Cognitive enhancement as a pharmacotherapy target for stimulant addiction. *Addiction*, **105**, 38-48.

Sun, H., Wu, H., Yu, X., Zhang, G., Zhang, R., Zhan, S., Wang, H., Bu, N., Ma, X. & Li, Y. (2015) Angiotensin II and its receptor in activated microglia enhanced neuronal loss and cognitive impairment following pilocarpine-induced status epilepticus. *Mol Cell Neurosci*, **65**, 58-67.

Tamarat, R., Silvestre, J.S., Durie, M. & Levy, B.I. (2002) Angiotensin II angiogenic effect in vivo involves vascular endothelial growth factor- and inflammation-related pathways. *Lab Invest*, **82**, 747-756.

Tan, H., Young, L.T., Shao, L., Che, Y., Honer, W.G. & Wang, J.F. (2012) Mood stabilizer lithium inhibits amphetamine-increased 4-hydroxynonenal-protein adducts in rat frontal cortex. *Int J Neuropsychoph*, **15**, 1275-1285.

Tesfamariam, B. & DeFelice, A.F. (2007) Endothelial injury in the initiation and progression of vascular disorders. *Vasc Pharmacol*, **46**, 229-237.

Thomas, D.M., Dowgiert, J., Geddes, T.J., Francescutti-Verbeem, D., Liu, X. & Kuhn, D.M. (2004) Microglial activation is a pharmacologically specific marker for the neurotoxic amphetamines. *Neurosci Lett*, **367**, 349-354.

Thomas, M., George, N.I., Patterson, T.A. & Bowyer, J.F. (2009) Amphetamine and environmentally induced hyperthermia differentially alter the expression of genes regulating vascular tone and angiogenesis in the meninges and associated vasculature. *Synapse*, **63**, 881-894.

Thomas, M., George, N.I., Saini, U.T., Patterson, T.A., Hanig, J.P. & Bowyer, J.F. (2010) Endoplasmic reticulum stress responses differ in meninges and associated vasculature, striatum, and parietal cortex after a neurotoxic amphetamine exposure. *Synapse*, **64**, 579-593.

Valvassori, S.S., Tonin, P.T., Varela, R.B., Carvalho, A.F., Mariot, E., Amboni, R.T., Bianchini, G., Andersen, M.L. & Quevedo, J. (2015) Lithium modulates the production of peripheral and cerebral cytokines in an animal model of mania induced by dextroamphetamine. *Bipolar Disord*, **17**, 507-517.

Villar-Cheda, B., Dominguez-Meijide, A., Valenzuela, R., Granado, N., Moratalla, R. & Labandeira-Garcia, J.L. (2014) Aging-related dysregulation of dopamine and angiotensin receptor interaction. *Neurobiol Aging*, **35**, 1726-1738.

Yabuki, Y., Shioda, N., Maeda, T., Hiraide, S., Togashi, H. & Fukunaga, K. (2014) Aberrant CaMKII activity in the medial prefrontal cortex is associated with cognitive dysfunction in ADHD model rats. *Brain Res*, **1557**, 90-100.

Yamamoto, B.K., Moszczynska, A. & Gudelsky, G.A. (2010) Amphetamine toxicities: classical and emerging mechanisms. *Ann NY Acad Sci*, **1187**, 101-121.

Yang, H.J., Wang, L., Cheng, Q. & Xu, H. (2011) Abnormal behaviors and microstructural changes in white matter of juvenile mice repeatedly exposed to amphetamine. *Schizoph Res Treatment*, **2011**, 542896.

Zhou, J., Ando, H., Macova, M., Dou, J. & Saavedra, J.M. (2005) Angiotensin II AT1 receptor blockade abolishes brain microvascular inflammation and heat shock protein responses in hypertensive rats. *J Cereb Blood Flow Metab*, **25**, 878-886.

Table 1. Astrocyte reactivity in infra-limbic prefrontal cortex.

	Saline		Amphetamine	
	GFAP+ AREA (%)	n	GFAP+ AREA (%)	n
Vehicle	1,62 ± 0,4	6	4,23 ± 0,69 *	6
Candesartan	1,82 ± 0,43	6	1,85 ± 0,12	6

The table shows astrocyte reactivity as GFAP positive area (%) in the four experimental groups, after the amphetamine challenge on day 17. Values are the mean±SEM; *different from control (p= 0.0041) and CV-Amph group (p= 0.0093).

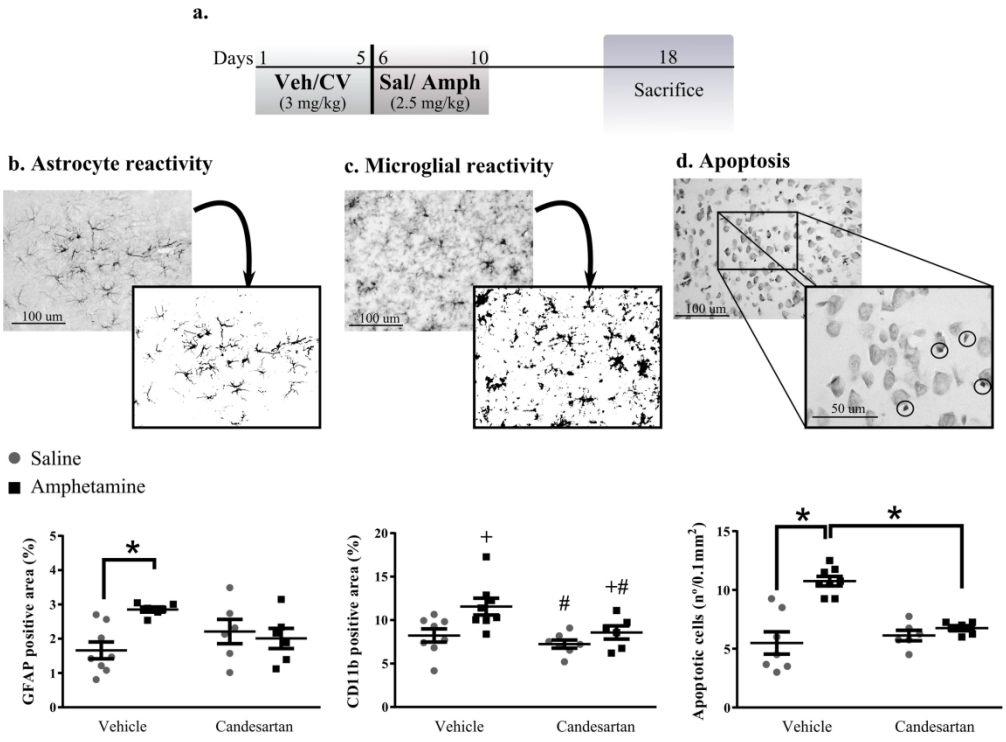

Fig. 1. Glial activation in pre-limbic prefrontal cortex. Schematic representation of the experimental protocol (a). The graphs show astrocyte reactivity by GFAP positive area (b), microglial activation by CD11b positive area (c) and the number of apoptotic cells by cresyl violet staining (d) in the four experimental groups. Values are the mean±SEM; *different from control group (p= 0.020) (b), # significant effect for treatment and + significant effect for drug (c), *different from control (p< 0.0001) and CV-Amph group (p= 0.0004) (c); n= 5-8.

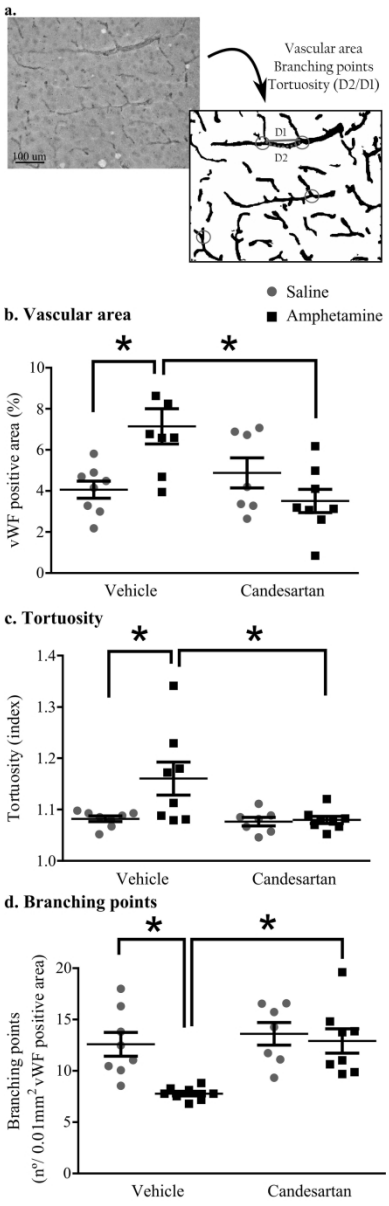

Fig. 2. Vascular network characteristics in prefrontal cortex. The microphotographs are representative of von Willebrand factor staining and show the parameters analyzed (a). Vascular network was evaluated considering: the percentage of vascular area (b), vessels' tortuosity (c) and the number of branching points (d). Values are the mean±SEM for the four experimental groups in basal conditions; *different from control (p= 0.014; p= 0.022; p= 0.010; for each parameter) and CV-Amph groups (p= 0.0030; p= 0.018; p= 0.0056; for each parameter), n= 7-8.

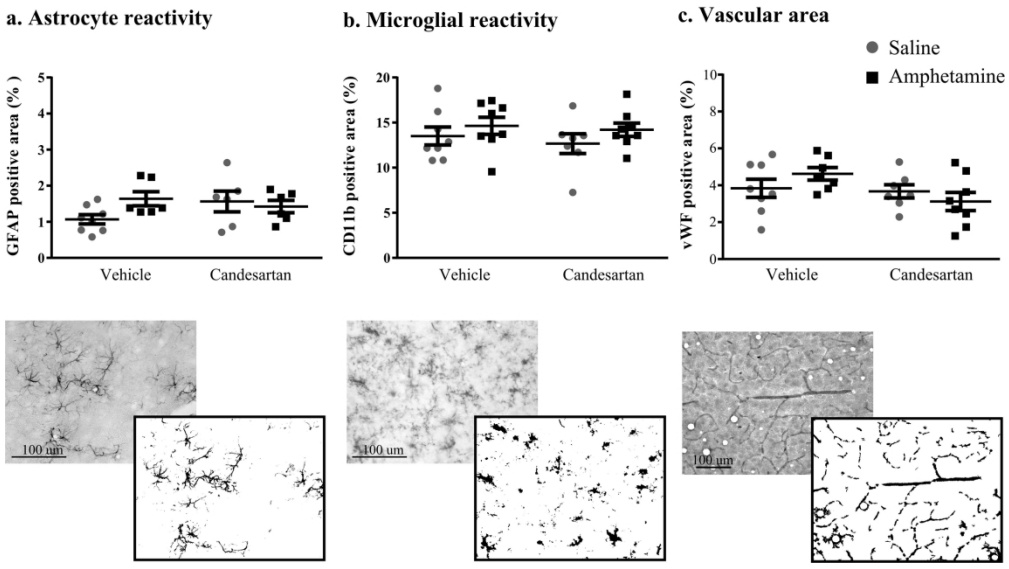

Fig. 3. Structural characteristics in infra-limbic prefrontal cortex. The graphs show GFAP positive area (n= 6-8) (a), CD11b positive area quantification (n=7-8) (b) and vascular network considering percentage of vascular area (n=7-8) (c). Values are the mean±SEM for the four experimental groups.

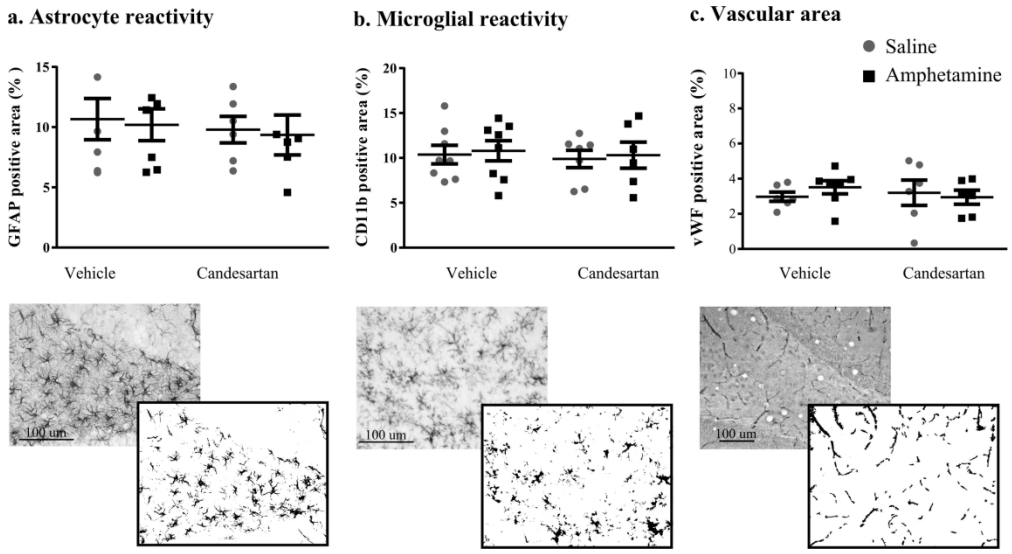

Fig. 4. Structural characteristics in hippocampus. The graphs show GFAP positive area (n= 5-8) (a), CD11b positive area quantification (n=6-8) (b) and vascular network considering percentage of vascular area (n=6-7) (c). Values are the mean±SEM for the four experimental groups.

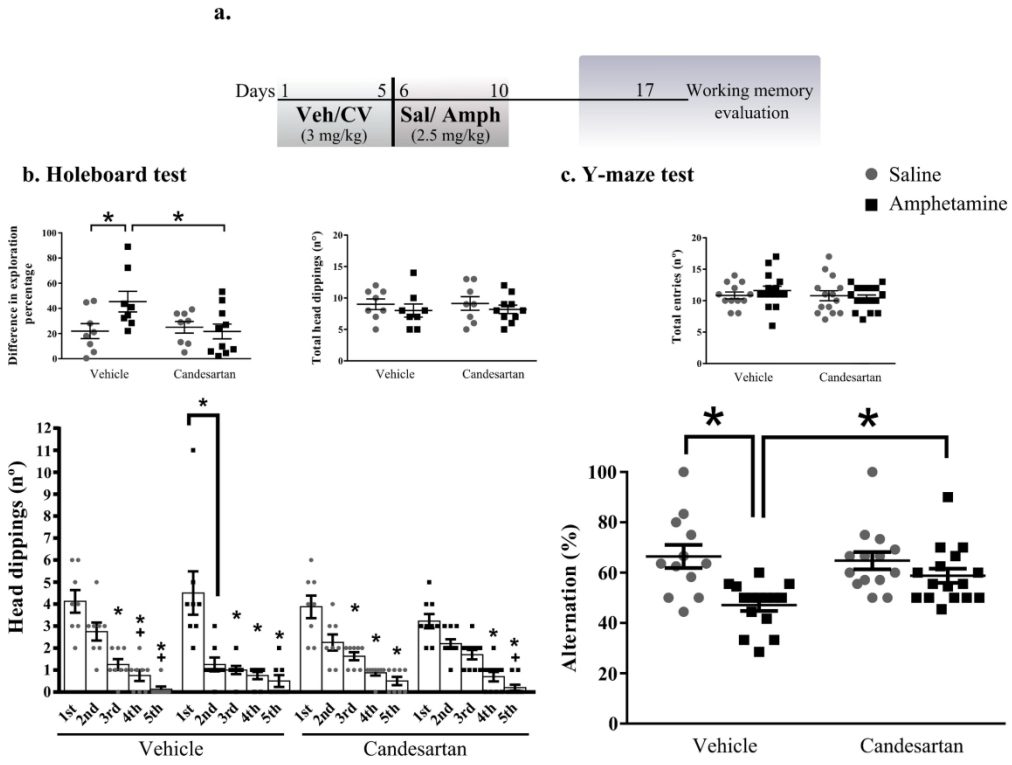

Fig. 5. Behavioral evaluation of attention performance- saline challenge. Schematic representation of the experimental protocol (a). Head dipping number during exploration in the holeboard test (n= 8-9). Hole exploration is ordered from the most to the least visited hole for each experimental group; * different from the most explored hole (1st) ($p<0.0001$). The left inset shows the difference in exploration percentage (%) between the two more explored holes; *different from control ($p=0.031$) and CV-Amph group ($p= 0.021$). The right inset shows the total head dipping (nº) during holeboard test (b). Percentage of alternations in the Y-maze test for the four experimental groups; *different from control ($p=0.0003$) and CV-Amph group ($p= 0.022$). The inset shows the total entries (nº) (n= 12-16) (c). Values are the mean±SEM.

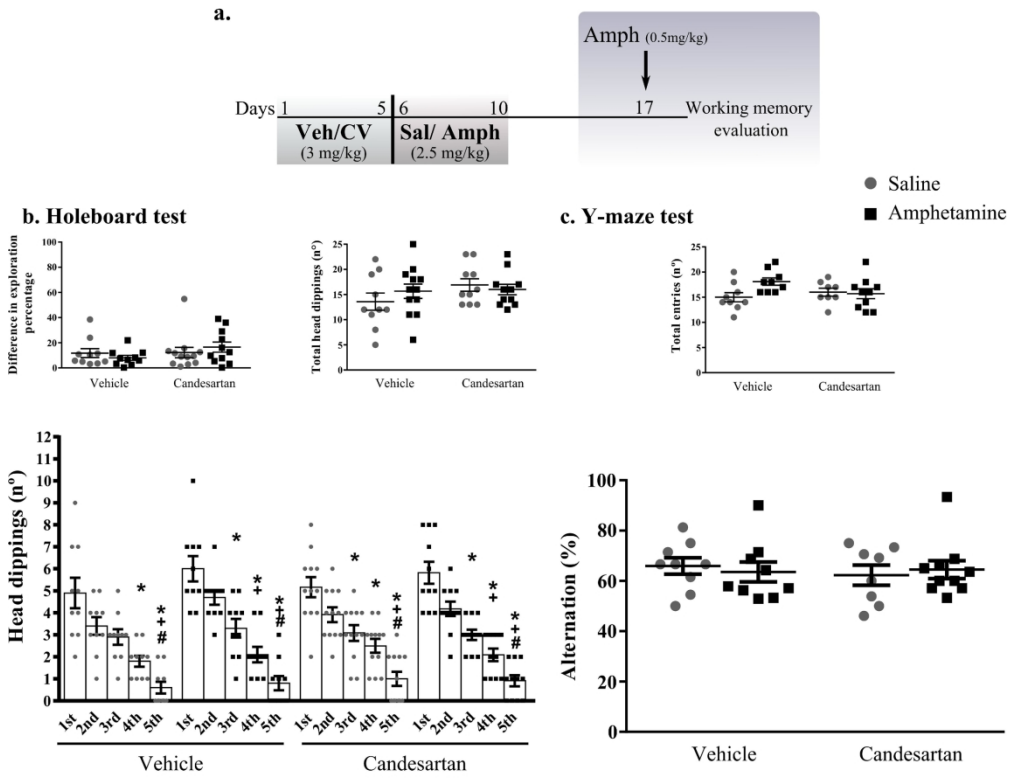

Fig. 6. Behavioral evaluation of attention performance- amphetamine challenge. Schematic representation of the experimental protocol (a). Head dipping number during exploration in the holeboard test (n= 10-12). The exploration to the holes is ordered from the most to the least visited hole for each experimental group. The left inset shows the difference in exploration percentage (%) between the two more explored holes. The right inset shows the total head dipping (nº) during holeboard test (b). Percentage of alternations in the Y-maze test for the four experimental groups, the inset shows the total entries (nº) (n= 8-10) (c). Values are the mean±SEM.

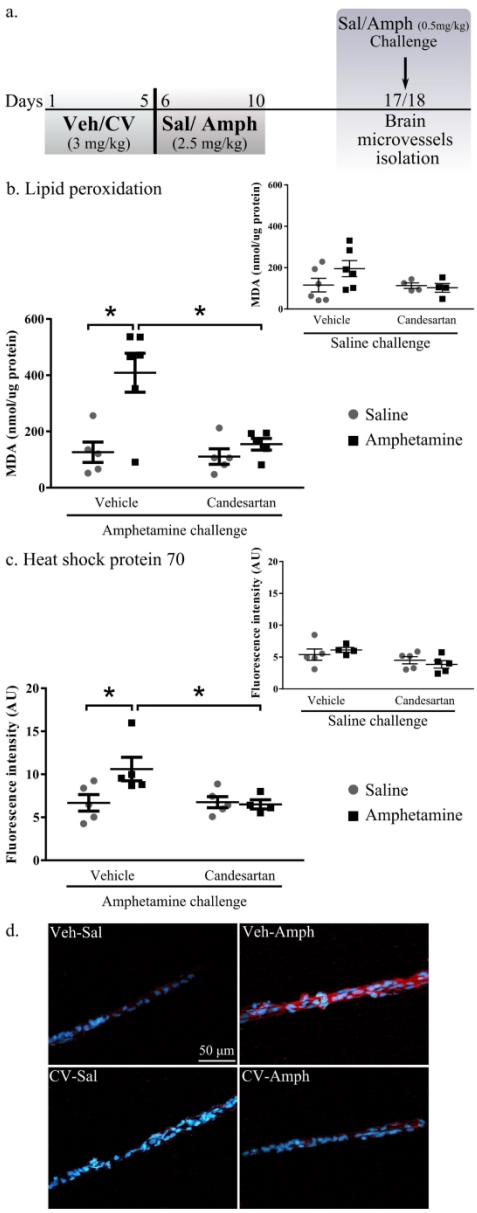

Fig. 7. Oxidative and cellular stress in brain microvessels. Schematic representation of the experimental protocol (a). The upper panel graphs show MDA levels in brain microvessels, in the four experimental groups, after the Amph challenge; *different from control (p= 0.0025) and CV-Amph group (p= 0.0065) (n=5-6). Unchanged values with saline challenge are shown in the inset, (n= 4-6) (b). HSP70 quantification after the Amph challenge; *different from control (p= 0.021) and CV-Amph group (p= 0.023) (n=4-5). Unchanged values with saline challenge are shown in the inset, (n= 4-5) (c). The microphotographs are representative of HSP70 expression in the four experimental groups receiving the Amph challenge (d). Values are the mean±SEM.